Vertical Structure of Upper-Ocean Seasonality: Extratropical Spiral versus Tropical Phase Lock

GE CHEN

Qingdao Collaborative Innovation Center of Marine Science and Technology, College of Information Science and Engineering, Ocean University of China, and Laboratory for Regional Oceanography and Numerical Modeling, Qingdao National Laboratory for Marine Science and Technology, Qingdao, China

XUAN WANG AND CHENGCHENG QIAN

Qingdao Collaborative Innovation Center of Marine Science and Technology, College of Information Science and Engineering, Ocean University of China, Qingdao, China

(Manuscript received 11 November 2015, in final form 21 March 2016)

ABSTRACT

Seasonality is a fundamental feature of the coupled ocean–atmosphere system. The hemispherically opposite general pattern at the air–sea interface is well known, but its penetrative behavior below the sea surface is poorly understood. Over 10 years of Argo data reveal for the first time the spiral-like structure of vertical seasonality in the upper extratropical ocean: the amplitude (strength of annual sea temperature variability) decreases rapidly with depth while the phase (peaking time) rotates from August (February) at the sea surface to December (June) at the bottom of the mixed layer in the Northern (Southern) Hemisphere under a clockwise representation. It is found that, analogous to the Ekman current spiral, the oceanic seasonality is almost reversed at approximately 500-m depth with about 5% of the surface intensity left. In contrast, the seasonality of subtropical oceans below the thermocline exhibits a phase-lock pattern around May and October to the north and south of the equator, respectively. Meanwhile, a systematic westward progression of annual phase corresponding to the warmest month is observed in the equatorial regions between 10°S and 10°N. It is suggested that the seasonality spiral of extratropical oceans occurs as a result of the vertical decay of solar penetration in tandem with delayed annual maximum mixing in the context of buoyancy and turbulent induced convections, while the month of full summer appears to be ''constant'' May (October) in the subtropical oceans of the Northern (Southern) Hemisphere under the stratified subsurface layer due to a 9-month trapping of penetrating solar energy from May (October) to next January (June). The vertically locked westward annual phase progression in the equatorial regions is likely to be a consequence of the first baroclinic mode of β-refracted annual Rossby waves. The spiral and phase-lock behaviors of the upper oceans are of critical significance to the understanding of mixed layer and thermocline dynamics.

1. Introduction

It is well known that seasonality on the globe is traditionally defined with temperature and is usually divided into a boreal pattern that peaks around August and an austral pattern that peaks around February (e.g., Sverdrup and Armbrust 2008; Roemmich and Gilson 2009). Such a global classification is naturally thought to be applicable to the ocean with perhaps a slight delay of the peaking time as a result of the higher heat capacity of the sea compared to the land. Generally, the oceanic seasonality is the largest component in sea surface temperature (SST) variability, which plays a critical role in air–sea interaction and global climate change.

The basic mechanism behind oceanic seasonality is associated with solar radiation, which has a dominant annual cycle with two special characteristics. First, heat is transferred to and from the ocean at the sea surface in hemispheric summer and winter, respectively (Chen et al. 2010). Second, a stronger seasonality in the Northern Hemisphere oceans is evident compared to its Southern Hemisphere counterparts due to the significant asymmetry of land–ocean distribution (Stine et al. 2009). It is

Corresponding author address: Ge Chen, College of Information Science and Engineering, Ocean University of China, 238 Songling Rd., Qingdao 266100, China.
E-mail: gechen@ouc.edu.cn

DOI: 10.1175/JCLI-D-15-0805.1

also understood that heat absorbed at the sea surface in hemispheric summer is transferred downward by buoyancy-forced convections and wind-, wave-, and/or current-generated turbulences (e.g., Shay and Gregg 1984; Boccaletti et al. 2004; Callaghan et al. 2014). While in hemispheric winter, heat is transferred upward toward the cooling surface. As a result, these processes with large spatiotemporal variations will transform the surface seasonality into the ocean interior with significant modifications (Chen and Wang 2016). In addition, the stabilizing effect by the ocean salinity stratification has been shown to be seasonally important at the base of the mixed layer above the main pycnocline in many places in the tropical oceans (Maes and O'Kane 2014).

Observations of the annual cycle in global upper-ocean temperature were very limited prior to the implementation of the Argo program (Giglio et al. 2013). A first basic description of the modern upper ocean based entirely on Argo data is presented by Roemmich and Gilson (2009), who examine the annual cycles of temperature, salinity, heat content, and steric height, and compare their results with other historical climatologies. With 2.5 years of underwater glider observations, the thermohaline fluctuations of the central subtropical North Pacific are estimated by Cole and Rudnick (2012). They point out that in the mixed layer, mesoscale and large-scale thermohaline structures usually have a significant annual cycle with the largest values near the surface and subtropical frontal regions. Using Argo data for the period 2005–12, Giglio et al. (2013) investigate the annual cycle in global steric height variability that includes diabatic changes in the surface layer due to air–sea buoyancy fluxes and adiabatic changes due to advection, which are dominant in the subsurface ocean. They find that in the subsurface ocean, Argo-derived steric height deviation over a season agrees with vertical advection of the mean potential density field by Ekman pumping, and the agreement extends beyond the tropics. Very recently, a detailed analysis of the three-dimensional (3D) structures of upper-ocean seasonality with emphasis on the vertical aspects of annual and semiannual cycles has been carried out by Chen and Wang (2016). Their main findings on vertical oceanic seasonality include midlatitude maxima in the near-surface layer, zonal "strips" in the subsurface layer, and systematic westward phase propagation in the intermediate layer. The existence of six eddy deserts as well as a dozen vertical quasi-annual amphidromes is also reported.

The present paper describes a twin work of Chen and Wang (2016), focusing on answering the following questions: 1) Do the seasons in the ocean interior have a systematic hemispheric opposition at all subsurface layers? 2) How do the oceanic seasons evolve with depth at a given location? 3) What are the geophysical mechanisms behind them? The answers to these questions are believed to be of tremendous importance to the understanding of climatic processes such as El Niño–Southern Oscillation under global warming and its hiatus, chemical processes such as nitrogen and carbon cycles in an oxygen-depleted environment, as well as biological processes such as phytoplankton blooms and fishery population shift, which all have a critical subsurface dimension (e.g., DelSole et al. 2014; Pörtner and Knust 2007; Ravichandran et al. 2012). The rest of the paper is organized as follows: a brief description of the Argo data and processing method is provided in section 2. The main results on vertical phase characteristics of the tropical and extratropical oceans are presented and analyzed in section 3. Potential mechanisms of the upper-ocean seasonality are discussed in section 4. Finally, several conclusions are given in section 5.

2. Data and method

In this study we use 11 years of Argo data spanning from 2004 to 2014 (Roemmich et al. 2009). By January 2016, there are as many as 3918 active floats disseminated around the global upper ocean (~0–2000 m). In this investigation, gridded Argo temperature data are obtained from the China Argo Real-Time Data Center (China Aerodynamics Research and Development Center 2013; http://www.argo.org.cn/). One is referred to section 2 of Chen and Wang (2016) for a detailed description of the data processing methodology, to their appendix A for the space–time interpolation schemes for Argo data reconstruction, and to their appendix B for the explained variance and significance level of the extracted annual and semiannual components from Argo-derived global ocean temperature.

3. Results

We first try to examine the penetrative behavior of seasonal signals into the upper ocean. The layer-averaged period-depth diagram of recovered amplitude of sea temperature variability within the intraannual band is shown in Fig. 1a. It is obvious that a multimode structure centered at 4, 6, 9, and 12 months can be identified throughout the global ocean, confirming previous findings that significant temperature variations exist below the thermocline on time scales ranging from intraseasonal (Matthews et al. 2007) to annual (Hosoda et al. 2006; Johnson 2011). As expected, the seasonal variation of sea temperature is dominated by the annual component, followed by the semiannual and intraseasonal components, with a rapidly decreasing intensity as going deeper for both hemispheres (Fig. 1b). Surprisingly, the annual, the semiannual, as well as the intraseasonal signals can all penetrate effectively into a depth of about 2000 m.

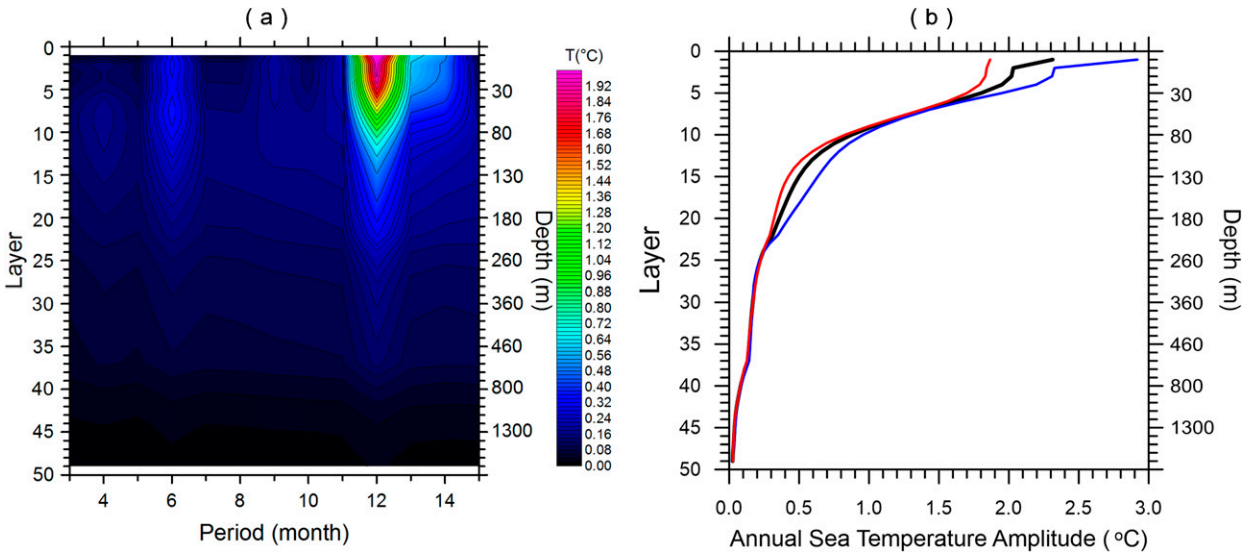

FIG. 1. (a) Period–depth diagram of layer-integrated spectrum of sea temperature variability for the seasonal band derived from Argo data of 2004–14. The color scale depicts the globally averaged harmonic amplitude of each depth layer. (b) Averaged annual amplitude of sea temperature (seasonality index) as a function of depth layer (corresponding to 0–2000 m) for the global (black), Northern Hemisphere (blue), and Southern Hemisphere (red) oceans. The kinks at layers 22 and 37 are due to the changes of vertical sampling interval of Argo floats from 10 to 20 m and from 20 to 100 m.

Next, we focus on the phase aspect of upper-ocean seasonality. As a point of departure, the histograms of annual sea temperature phase distribution (i.e., the month in which the temperature peaks at a given location) at selected depths for the extratropical and tropical oceans are shown in Fig. 2. As far as the latitude band of 30°–60°N is concerned (Fig. 2a), the month of full summer appears to have a gradual delay with increasing depth: shifting from August at the sea surface to December at about 340 m. A similar pattern can also be observed for its Southern Hemisphere counterpart between 30° and 60°S with an austral full summer in February at the sea surface while in June at about 340 m (Fig. 2b). As for the top 150 m of the tropical oceans, the seasonality largely follows the extratropical pattern of their hemisphere with a much weaker annual cycle (not shown). Between around 150 m and over 1000 m, however, the season of full boreal (austral) summer appears to be largely in April–May (October–November), exhibiting a notable feature of vertical phase lock for the tropical oceanic seasonality (Fig. 2c). Farther downward to about 2000 m, it is difficult to identify any coherent seasonal cycle given the flat nature of the phase histogram (not shown).

It should be pointed out that the spread of the deeper phase histograms may be partially due to the phase locking onto the month of large eddies. Since mesoscale eddies can trap fluid parcels within the eddy core and transport them discretely, the matching between eddy property and oceanic seasonality in terms of spatiotemporal scale and geographical location has been demonstrated, especially within the zone of 500 ± 300-m depths at a semiannual periodicity [the so-called space–time ''windows'' for detecting eddy signatures via Argo-derived temperature amplitude and phase (see Chen and Wang 2016)]. The ''contamination'' effect of mesoscale eddies on oceanic seasonality at their dominant depths and frequencies is an interesting topic for future study.

Analogous to the Ekman current, the rotational behavior of the extratropical oceanic seasonality can also be intuitively illustrated using a chart of spiral with the length of the arrow being proportional to the amplitude of annual temperature variation at each depth layer, and the direction of the arrow being the peaking month of hemispheric summer following a clockwise representation as shown in Figs. 3a and 3b for the Northern and Southern Hemisphere, respectively. It is found that, similar to the Ekman current spiral (see, e.g., Sverdrup and Armbrust 2008), the oceanic seasonality is almost reversed at about 500 m (~400 m) depth in the Northern (Southern) Hemisphere with only approximately 2.6% (~7.0%) of the surface intensity left, suggesting that when summer is active at a given location in the surface layer, winter is approaching at the same location several hundreds of meters beneath. It should be pointed out, however, that systematic seasonal signatures in terms of hemispheric phase consistency start to disappear below 500 m, although localized seasonality remains significant down to at least 2000-m depth in the ocean (see Fig. 1).

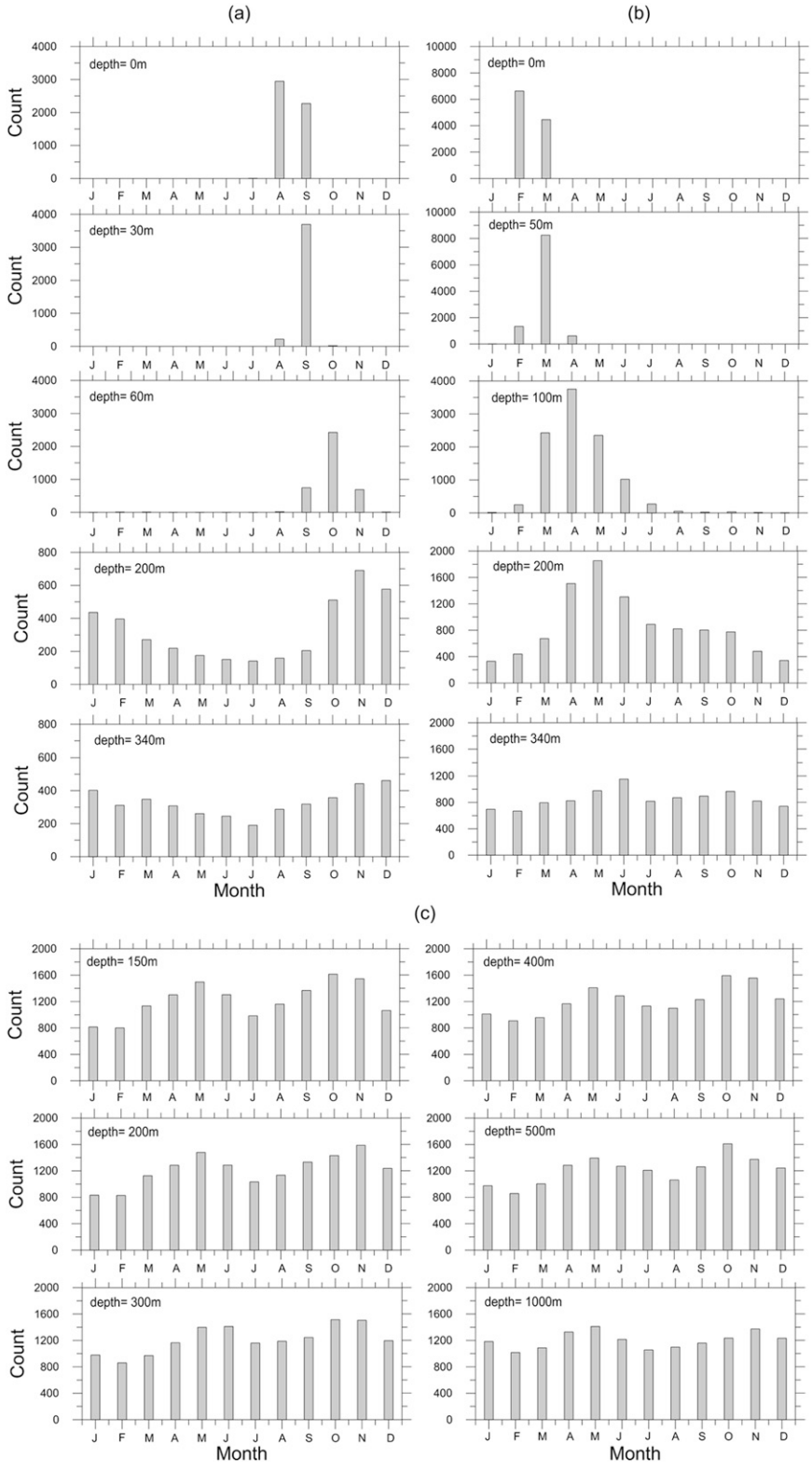

FIG. 2. Histograms of annual sea temperature phase distribution at selected depths for (a) the northern extratropical oceans (30°–60°N at 0, 30, 60, 200, and 340 m), (b) the southern extratropical oceans (30°–60°S at 0, 50, 100, 200, and 340 m), and (c) the tropical oceans (30°–30°N at 150, 200, 300, 400, 500, and 1000 m).

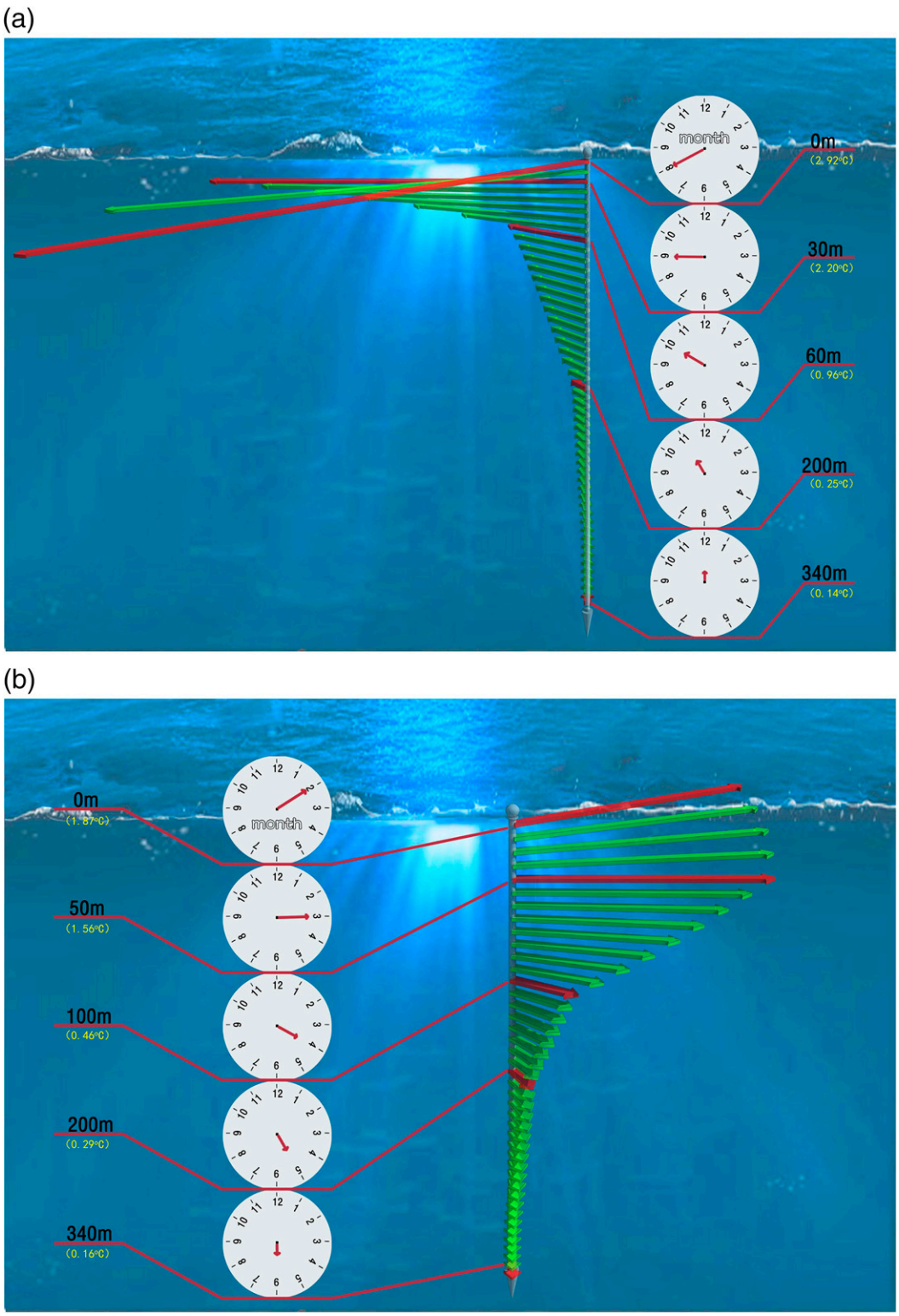

FIG. 3. The seasonality spiral of the (a) Northern and (b) Southern Hemisphere extratropical oceans expressed in maximum likelihood (in terms of peaking month) of recovered annual phase of sea temperature variability with respect to depth. The length of the arrow at each depth layer is proportional to the strength of corresponding sea temperature seasonality, and the annual temperature amplitudes at selected depths are labeled in yellow. The right-hand side in (a) and left-hand side in (b) show the clockwise projections of the spirals at selected depths.

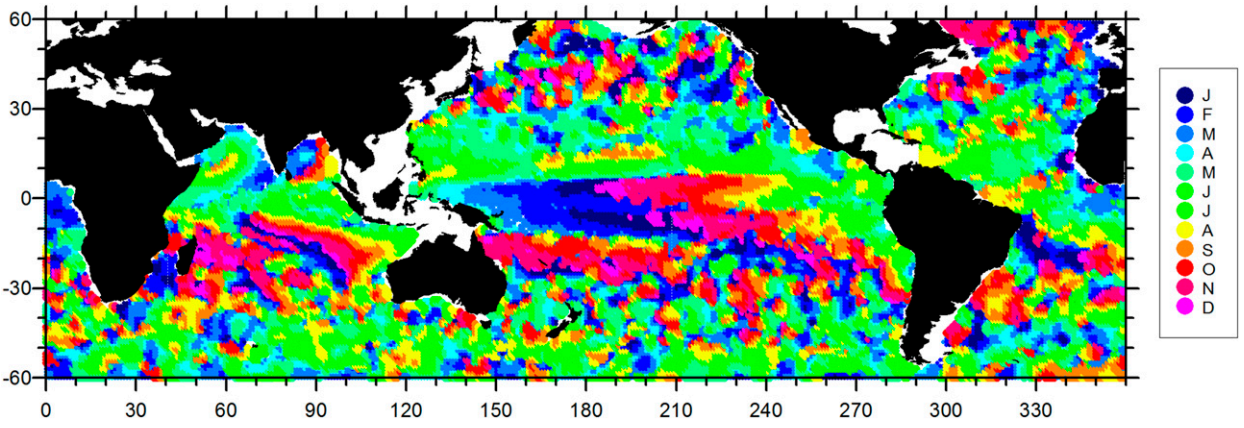

FIG. 4. Map of vertically averaged annual phase of the global oceans between 120 and 1300 m.

To further reveal the phase-lock nature of the tropical oceanic seasonality, a map of vertically averaged annual phase between 120 and 1300 m corresponding to the month of peak warmth is shown in Fig. 4 (note that no significant change can be found if a smaller depth range is used, indicating that the general pattern is rather stable). It is apparent that hemispheric reversal of season can only be observed between the zonal bands of 10°–30°S and 10°–30°N. Within the equatorial region between 10°S and 10°N, the phase pattern is characterized by a systematic westward annual propagation across the Pacific and Indian Oceans, but to a lesser extent in the Atlantic Ocean. Meanwhile, it is also clear that the phase distribution displays a localized random picture at these depths in the extratropical oceans of the two hemispheres.

4. Discussion

a. *Extratropical spiral*

As the extratropical seasonality spiral mainly exist within the upper hundreds of meters of the ocean, coinciding with the zone of active seasonal mixing (e.g., Brainerd and Gregg 1995; Chen and Yu 2015), its formation has to be understood in the context of ventilation dynamics driven by solar-induced buoyancy forcing and wind- and/or wave-induced turbulent forcing on both daily and yearly basis, as shown in the conceptual schematic in Fig. 5. We first concentrate on a typical diurnal cycle of convection and stratification. In early autumn, a daily convection starts to intensify by increasing nighttime cooling in the early evening. During this period, the ocean loses heat to the atmosphere and potential energy is converted to turbulent kinetic energy. As described by Callaghan et al. (2014), this drives convective overturns that result in the deepening of the diurnal thermocline entraining more quiescent water upward from below. The diurnal thermocline typically reaches its daily maximum depth at the transition between nighttime cooling and daytime heating when the surface heat flux reverses sign. The convective forcing eventually ends in the morning, and the turbulence through most of the depth of the mixed layer starts to decay. Soon thereafter, a shallow warm layer begins to form (corresponding to the height of turbulence zone near the surface). After midday, the diurnal thermocline is growing in strength, on top of which a shallow restratified layer is formed with a relatively warm temperature.

At this point, it is helpful to recall some of the early works on observation and modeling of diurnal cycles of upper-ocean temperature and heat content. To document the effect of late summer–early fall episodes on the upper ocean and to study the erosion of the mixed layer into the top of the seasonal thermocline, a cooperative Mixed Layer Experiment (MILE) was staged during August and September 1977, in the vicinity of Ocean Weather Station P (50°N, 145°W) (Davis et al. 1981). They point out that "The low frequency temperature changes of the upper ocean, including erosion of initial stratification, lifting (or cooling) of the seasonal thermocline, net warming of the entire upper layer, and gradual subsidence of the seasonal thermocline are clearly observed. In particular, high-frequency internal wave events are identified in the seasonal thermocline" (Davis et al. 1981, p. 1427). A few years later, measurements from Research Platform (R/P) *Floating Instrument Platform* (*FLIP*) off San Diego, California, are used by Price et al. (1986) to have a detailed look at the diurnal cycle of the upper ocean. They conclude that

> "The diurnal cycle is an important mode of fair weather variability which arises when solar heating stabilizes the surface layer and causes the surface fluxes of heat and momentum to be surface trapped during midday. Heat and momentum fluxes appear to be mixed in a similar way, so that the thermal and velocity cycles are closely coupled. Temperature and velocity profiles observed

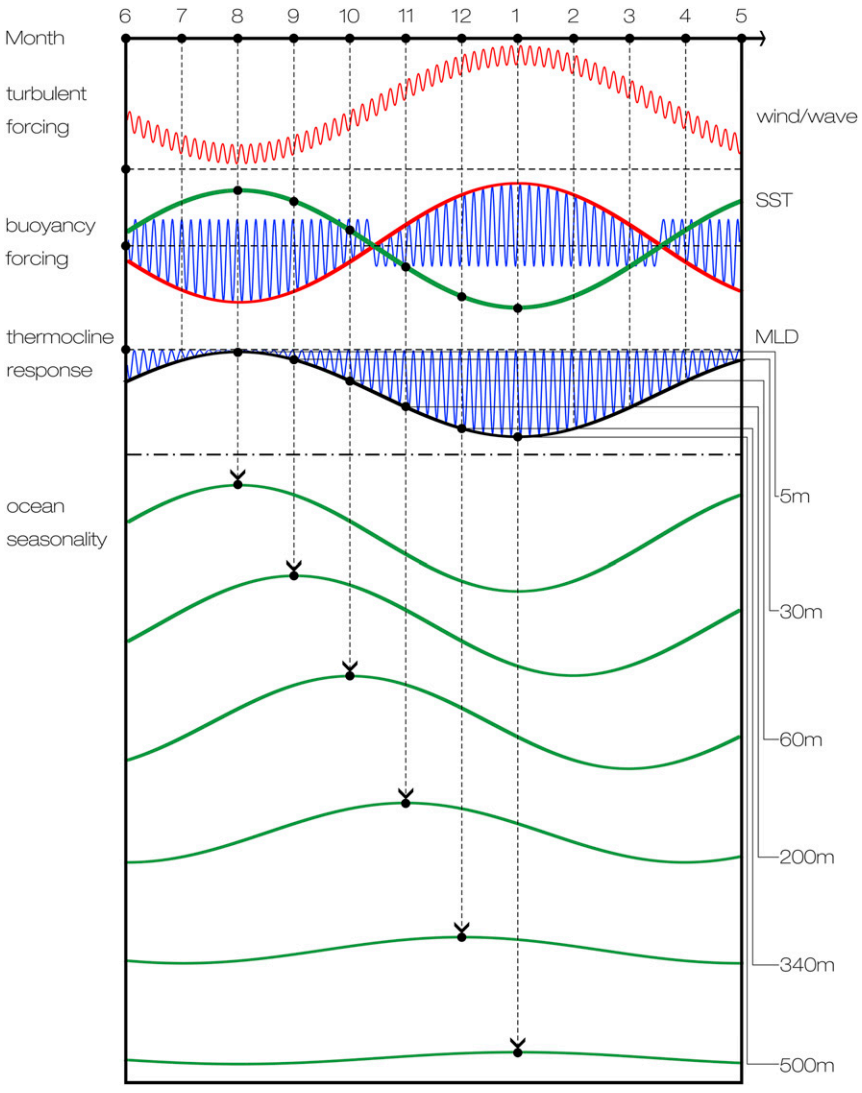

FIG. 5. A conceptual schematic of convection dynamics leading to the seasonality spiral of the Northern Hemisphere extratropical oceans. The buoyancy forcing by solar heating (thin red) and turbulent forcing by wind and wave (thick red), as well as thermocline response in terms of MLD (black) and oceanic seasonality responses at different depths (green) are illustrated on diurnal (high frequency) and annual (low frequency) cycles. Note that the progression of peaking month and its corresponding temperature maximum are indicated vertically by dashed arrow lines.

during the afternoon often show a two-layer structure, with coincident temperature and velocity surface mixed layers overlying a thick, stratified and sheared transition layer'' (Price et al. 1986, p. 8424).

Wind mixing causes a pronounced asymmetry of the temperature response by limiting the warming phase to only about half of the period that the surface heat flux is positive. Moored observations of atmospheric variables and upper-ocean temperatures from the Long-Term Upper-Ocean Study (LOTUS) and the Frontal Air–Sea Interaction Experiment (FASINEX) are also used to examine the upper-ocean response to surface heating (Lee and Rudnick 1996). They reveal that mixing dominates the balance over a given penetration depth, below which vertical advection becomes important and the sense of phase propagation reverses. In addition, they mention that the time-averaged profile of wind-driven velocity that makes up the Ekman transport has a flat, spiral shape as a direct consequence of diurnal cycling. Observations during the MILE (Davis et al. 1981), the LOTUS (Price et al. 1987), and the FASINEX (Lee and Rudnick 1996) have all verified the Ekman transport relationship and characterized the vertical momentum flux as a wind-driven current spiral.

Keeping the above understandings in mind, it is obvious that the process of diurnal cycle plays an important role in shaping the long-term response of the upper ocean to atmospheric forcing. When the upper ocean is in a situation of net heat loss to the atmosphere on time scales of a few days or more, one can expect a gradually enhanced daily alternation between convection at night and restratification during the day. The depth of the seasonal thermocline is the cumulative effect of these convective deepenings. As time goes on from September to the following January in the Northern Hemisphere, one finds a gradually deepening seasonal mixed layer that transmits and homogenizes the slowly decreasing sea surface temperature to the top of the seasonal thermocline through the mixed water column. This process is considerably amplified by the turbulent forcing from winds and waves in terms of Langmuir circulation whose overall intensity follows a similar seasonal cycle. These effects combine to explain the time lag and peak temperature decline (corresponding to a delayed and weakened summer) with an increasing depth, resulting in the spiral structure of oceanic seasonality as revealed by Argo data (Fig. 3). The angular velocity is estimated to be roughly $1^\circ\,\mathrm{day}^{-1}$, equivalent to a penetrating speed of 2–3 $\mathrm{m\,day}^{-1}$ (see also Fig. 5).

b. *Tropical phase lock*

The phase lock of tropical oceanic seasonality below the thermocline is seen to have a general three-band structure: a near-constant May full summer for 10°–30°N (the northern trade wind zone), a largely October full summer for 10°–30°S (the southern trade wind zone), and a westward annual propagation pattern in the equatorial regions between 10°S and 10°N (Fig. 4). It is understood that solar radiation can penetrate beyond the base of the oceanic mixed layer through its vertical divergence, and directly heat well below the ocean surface. According to Ohlmann et al. (1996), solar radiation penetration can be a significant term ($20\,\mathrm{W\,m}^{-2}$) in the mixed layer heat budget for the tropical regions. Moreover, annual cycles in incident solar flux, upper-ocean chlorophyll and pigment concentrations, and mixed layer depth (MLD) can cause trapping of penetrating solar energy of $O(10)\,\mathrm{W\,m}^{-2}$ within the seasonal pycnocline. This trapped thermal energy is unavailable for atmospheric exchange until full winter—a period as long as nine months from May (October) to the next January (June) as far as the Northern (Southern) Hemisphere is concerned. Or in other words, summer peak below the thermocline is ''fixed'' to May (October) for the northern (southern) tropical ocean as observed in Fig. 2c. This argument is also consistent with the recent findings of Schiller and Ridgway (2013) that local cooling (warming) in the mixed layer proceeds maxima (minima) in MLD (and hence the underthermocline season) by as much as three months.

In contrast to the near-constant phase lock below the trade wind zones of the two hemispheres, the underthermocline seasonality within the core equatorial regions (10°S–10°N) has an annual cycle from May in the east to December in the central region, and to April in the west of the Pacific Ocean, as well as the Atlantic and Indian Oceans though less well defined (Fig. 4). The westward-propagating tongue-shaped signature of the thermal phase coincides fairly well with the β-refracted Rossby wave revealed by satellite sea surface height data (Chelton and Schlax 1996). As understood, an important feature of the first baroclinic mode of Rossby wave is that variations of the sea surface height are mirrored as thermocline depth variations of the opposite sign with about three orders of magnitude greater amplitude (Gill 1982). As a result, such large variations of subsurface wave propagation is obviously a major force in shaping the seasonality pattern below the thermocline, especially for the equatorial regions where the peaks of tropical Rossby waves are found [4°S and 4°N, see Fig. 3 of Chelton and Schlax (1996)].

5. Conclusions

Based on 11 years of high-quality Argo data for the period of 2004–14, the 3D structures of upper-ocean seasonality are revealed in details. The formation mechanisms of their vertical characteristics are explored in the context of convection/advection and Rossby wave dynamics. The main conclusions are summarized below.

First, the 3D seasonality of the extratropical oceans in the two hemispheres can be intuitively characterized by a pseudospiral down to a depth of approximately 500 m, where the four seasons are almost reversed with respect to the sea surface along with an intensity reduction of about 95%. Convections on diurnal and annual basis are believed to be the most important mechanism by which heat is transferred between the sea surface and the thermocline. Direct atmospheric forcing of the upper ocean is also produced by the work of wind stress and wave action. As the combined buoyancy and turbulent mixing may last for nearly half a year at midlatitudes, the season opposition between the air–sea interface and the maximum annual mixed layer depth (Chen and Yu 2015) can be naturally expected.

Second, the season below the annual thermocline in the tropical oceans is found to be generally phase locked. This is because the intensity of solar radiation

remains fairly constant at tropical latitudes over the year, given that the sun's noontime rays are always received at an angle approaching 90° and the length of the daylight period is nearly constant (Sverdrup and Armbrust 2008). Therefore, the season of summer appears to be locked to May (October) in the subtropical oceans of the Northern (Southern) Hemisphere under the stratified subsurface layer due to the nine-month trapping of penetrating solar energy from May (October) to the next January (June).

Third, the near-constant phase lock of oceanic seasons appears to be violated in the equatorial region between 10°S and 10°N. Instead, a systematic westward annual progression of the warmest months is observed in all three ocean basins with a leading tip along the equator. This tongue-shaped bending of thermal phase is highly consistent with the property of the first baroclinic mode of β-refracted annual Rossby waves. Since Rossby waves of this kind are common in this region (Chelton and Schlax 1996), and the corresponding variations of sea surface height may lead to tremendously greater amplitudes in thermocline depth variations, it is therefore argued that the persistent internal stirring by annual baroclinic Rossby waves is likely to play a decisive role in determining the vertical pattern of equatorial oceanic seasonality.

Acknowledgments. This research was jointly supported by the Natural Science Foundation of China under Grants 41331172, U1406404, and 61361136001, the Global Change Research Program of China under Grant 2012CB955603, and the Scientific and Technological Innovation Project of the Qingdao National Laboratory for Marine Science and Technology under Grant 2015ASKJ01. Special thanks go to the China Argo Real-Time Data Center for providing us with the gridded Argo data product used in this study.

REFERENCES

Boccaletti, G., R. C. Pacanowski, S. G. H. Philander, and A. V. Fedorov, 2004: The thermal structure of the upper ocean. *J. Phys. Oceanogr.*, **34**, 888–902, doi:10.1175/1520-0485(2004)034<0888:TTSOTU>2.0.CO;2.

Brainerd, K. E., and M. C. Gregg, 1995: Surface mixed and mixing layer depths. *Deep-Sea Res. I*, **42**, 1521–1543, doi:10.1016/0967-0637(95)00068-H.

Callaghan, A. H., B. Ward, and J. Vialard, 2014: Influence of surface forcing on near-surface and mixing layer turbulence in the tropical Indian Ocean. *Deep-Sea Res. I*, **94**, 107–123, doi:10.1016/j.dsr.2014.08.009.

China Aerodynamics Research and Development Center, 2013: User manual of gridded Argo data (in Chinese). China Aerodynamics Research and Development Center, Hangzhou, China, 31 pp.

Chelton, D. B., and M. G. Schlax, 1996: Global observations of oceanic Rossby waves. *Science*, **272**, 234–238, doi:10.1126/science.272.5259.234.

Chen, G., and F. Yu, 2015: An objective algorithm for estimating maximum oceanic mixed layer depth using seasonality indices derived from Argo temperature/salinity profiles. *J. Geophys. Res. Oceans*, **120**, 582–595, doi:10.1002/2014JC010383.

——, and X. Wang, 2016: Vertical structure of upper-ocean seasonality: Annual and semiannual cycles with oceanographic implications. *J. Climate*, **29**, 37–59, doi:10.1175/JCLI-D-14-00855.1.

——, B. Shao, Y. Han, J. Ma, and B. Chapron, 2010: Modality of semiannual to multidecadal oscillations in global sea surface temperature variability. *J. Geophys. Res.*, **115**, C03005, doi:10.1029/2009JC005574.

Cole, S. T., and D. L. Rudnick, 2012: The spatial distribution and annual cycle of upper ocean thermohaline structure. *J. Geophys. Res.*, **117**, C02027, doi:10.1029/2011JC007033.

Davis, R. E., R. deSzoeke, D. Halpern, and P. Niiler, 1981: Variability in the upper ocean during MILE. Part I: The heat and momentum balances. *Deep-Sea Res.*, **28A**, 1427–1451, doi:10.1016/0198-0149(81)90091-1.

DelSole, T., X. Yan, P. A. Dirmeyer, M. Fennessy, and E. Altshuler, 2014: Changes in seasonal predictability due to global warming. *J. Climate*, **27**, 300–311, doi:10.1175/JCLI-D-13-00026.1.

Giglio, D., D. Roemmich, and B. Cornuelle, 2013: Understanding the annual cycle in global steric height. *Geophys. Res. Lett.*, **40**, 4349–4354, doi:10.1002/grl.50774.

Gill, A. E., 1982: *Atmosphere–Ocean Dynamics*. Academic Press, 662 pp.

Hosoda, S., S. Minato, and N. Shikama, 2006: Seasonal temperature variation below the thermocline detected by Argo floats. *Geophys. Res. Lett.*, **33**, L13604, doi:10.1029/2006GL026070.

Johnson, G. C., 2011: Deep signatures of southern tropical Indian Ocean annual Rossby waves. *J. Phys. Oceanogr.*, **41**, 1958–1964, doi:10.1175/JPO-D-11-029.1.

Lee, C. M., and D. L. Rudnick, 1996: The upper-ocean response to surface heating. *J. Phys. Oceanogr.*, **26**, 466–480, doi:10.1175/1520-0485(1996)026<0466:TUORTS>2.0.CO;2.

Maes, C., and T. J. O'Kane, 2014: Seasonal variations of the upper ocean salinity stratification in the Tropics. *J. Geophys. Res. Oceans*, **119**, 1706–1722, doi:10.1002/2013JC009366.

Matthews, A. J., P. Singhruck, and K. J. Heywood, 2007: Deep ocean impact of a Madden-Julian Oscillation observed by Argo floats. *Science*, **318**, 1765–1769, doi:10.1126/science.1147312.

Ohlmann, J. C., D. A. Siegel, and C. Gautier, 1996: Ocean mixed layer radiant heating and solar penetration: A global analysis. *J. Climate*, **9**, 2265–2280, doi:10.1175/1520-0442(1996)009<2265:OMLRHA>2.0.CO;2.

Pörtner, H. O., and R. Knust, 2007: Climate change affects marine fishes through the oxygen limitation of thermal tolerance. *Science*, **315**, 95–97, doi:10.1126/science.1135471.

Price, J. F., R. A. Weller, and R. Pinkel, 1986: Diurnal cycling: Observations and models of the upper ocean response to diurnal heating, cooling, and wind mixing. *J. Geophys. Res.*, **91**, 8411–8427, doi:10.1029/JC091iC07p08411.

——, ——, and R. R. Schudlich, 1987: Wind-driven ocean currents and Ekman transport. *Science*, **238**, 1534–1538, doi:10.1126/science.238.4833.1534.

Ravichandran, M., M. S. Girishkumar, and S. Riser, 2012: Observed variability of chlorophyll-a using Argo profiling floats in the southeastern Arabian Sea. *Deep-Sea Res. I*, **65**, 15–25, doi:10.1016/j.dsr.2012.03.003.

Roemmich, D., and J. Gilson, 2009: The 2004-2008 mean and annual cycle of temperature, salinity, and steric height in the

global ocean from the Argo Program. *Prog. Oceanogr.*, **82**, 81–100, doi:10.1016/j.pocean.2009.03.004.

——, and Coauthors, 2009: The Argo program observing the global ocean with profiling floats. *Oceanography*, **22**, 34–43, doi:10.5670/oceanog.2009.36.

Schiller, A., and K. R. Ridgway, 2013: Seasonal mixed-layer dynamics in an eddy-resolving ocean circulation model. *J. Geophys. Res. Oceans*, **118**, 3387–3405, doi:10.1002/jgrc.20250.

Shay, T. J., and M. C. Gregg, 1984: Turbulence in an oceanic convective mixed layer. *Nature*, **310**, 282–285, doi:10.1038/310282a0.

Stine, A. R., P. Huybers, and I. Y. Fung, 2009: Changes in the phase of the annual cycle of surface temperature. *Nature*, **457**, 435–440, doi:10.1038/nature07675.

Sverdrup, K. A., and V. Armbrust, 2008: *An Introduction to the World's Oceans*. 10th ed. McGraw Hill Higher Education, 528 pp.